DNA damage-induced EMT controlled by the PARP dependent chromatin remodeler ALC1 promotes DNA repair efficiency through RAD51 in tumor cells

Fatemeh Rajabi, Rebecca Smith, Win-Yan Liu-Bordes, Michael Schertzer, Sebastien Huet, Arturo Londoño-Vallejo

DNA damage-induced EMT controlled by the PARP dependent chromatin remodeler ALC1 promotes DNA repair efficiency through RAD51 in tumor cells

Fatemeh Rajabi[1,3,*], Rebecca Smith[2,4], Win-Yan Liu-Bordes[1], Michael Schertzer[1], Sebastien Huet[2], Arturo Londoño-Vallejo[1,5,*]

[1] Institut Curie, CNRS-UMR3244, Sorbonne University, 75005 Paris, France.

[2] Univ Rennes, CNRS, IGDR (Institut de génétique et développement de Rennes) - UMR 6290, BIOSIT – UMS3480, F- 35000 Rennes, France.

[3] Present address: Cancer Genomics lab, Inserm-U981, Gustave Roussy Cancer Center Grand Paris, Villejuif, 94805, France.

[4] Present address: Sir William Dunn School of Pathology, University of Oxford, South Parks Road, Oxford, OX1 3RE, UK.

[5] Present address: Institut Curie, Inserm U1021-CNRS UMR 3347, Paris Saclay University, Centre Universitaire, 91405 Orsay Cedex, France.

[*]Corresponding authors: Jose-Arturo.Londono-Vallejo@curie.fr & Fatemeh.rajabi@gustaveroussy.fr

Keywords: EMT, DDR, PARP, ALC1, RAD51.

ABSTRACT

Epithelial-to-mesenchymal transition (EMT) allows cancer cells to metastasize while acquiring resistance to apoptosis and chemotherapeutic agents with significant implications for patients' prognosis and survival. Despite its clinical relevance, the mechanisms initiating EMT during cancer progression remain poorly understood. We demonstrate that DNA damage triggers EMT and that activation of PARP and the PARP-dependent chromatin remodeler ALC1 (CHD1L) was required for this response. Our results suggest that this activation directly facilitates access to the chromatin of EMT transcriptional factors (TFs) which then initiate cell reprogramming. We also show that EMT-TFs bind to the RAD51 promoter to stimulate its expression and to promote DNA repair by homologous recombination (HR). Importantly, a clinically relevant PARP inhibitor reversed or prevented EMT in response to DNA damage while resensitizing tumor cells to other genotoxic agents. Overall, our observations shed light on the intricate

relationship between EMT, DNA damage response, and PARP inhibitors, providing potential insights for in cancer therapeutics.

INTRODUCTION

The Epithelial-to-Mesenchymal Transition (EMT) is a developmental process that sustains organogenesis allowing embryonic progenitor epithelial cells to migrate and colonize new niches, where cells undergo the reverse process (mesenchymal-to-epithelial transition, MET) and final differentiation (reviewed in (Derynck and Weinberg, 2019)). This phenomenon is governed by six transcriptional factors that trigger global changes in gene expression, driving major cytoskeleton reorganization and conferring cell mobility properties (Stemmler *et al.*, 2019). In adult organisms, a similar program occurs during physiological healing processes but also during tumor progression. Indeed, EMT has been linked to the metastatic process, as well as with the acquisition of stem-like properties and resistance to chemotherapeutic agents by tumor cells (Puisieux *et al.*, 2014; Pastushenko and Blanpain, 2019). Multiple pathways have been shown to modulate the EMT program in cancer cells, but little is known about the mechanisms responsible for initiating EMT in the primary tumor. Previous work in our laboratory (Castro-Vega *et al.*, 2013; Castro-Vega *et al.*, 2015) has shown that persistent endogenous DNA damage resulting from repeated telomere-driven breakage-fusion-bridge cycles promotes EMT in transformed human epithelial kidney (HEK) cells. This observation suggested that EMT may occur in early carcinoma cells exhibiting chromosome instability (CIN) (Shih *et al.*, 2001; Maser and DePinho, 2002; Rajagopalan and Lengauer, 2004). Notably, an EMT-compatible signature has been detected in experimental models of metastatic cancer in association with CIN (Bakhoum *et al.*, 2018).

CIN stands out as one of the most pervasive hallmarks of cancer cells (Nowak *et al.*, 2002). Direct evidence supporting its contribution to tumorigenesis has come from clinical observations associating inherited mutations in genes involved in genome maintenance and DNA repair with an elevated risk for carriers to develop carcinomas (Lynch *et al.*, 2004; Wolters and Schumacher, 2013; Kass *et al.*, 2016). A paradigmatic example of this association is found in BRCA1/2 constitutive mutations, correlating with an increased susceptibility to breast and ovarian cancers (Romero-Laorden and Castro, 2017). Furthermore, in different carcinomas, there is a direct correlation between the degree of CIN in the primary tumor and the increased risk of death attributed to metastatic disease (Taylor *et al.*, 2010; Watanabe *et al.*, 2012). Despite the clinical significance of CIN in cancer progression, the molecular mechanisms linking CIN to the ability of tumors to metastasize in vivo are not fully understood. These connections likely encompass both cell-autonomous mechanisms, such as the inflammatory response triggered by the detection of double-stranded DNA in the cytoplasm (Bakhoum *et al.*, 2018), as well as cell non-autonomous ones, such as a local senescent or pro-inflammatory microenvironment (Castro-Vega *et al.*, 2015; Ortiz-Montero *et al.*, 2017; Harper *et al.*, 2018).

Multiple molecular connections between EMT and the response to DNA damage (DDR) have already been described. For instance, inhibition of ATR leads to increased expression of ZEB1, a major EMT transcriptional factor (EMT-TF) and preventing ZEB1 expression in this context leads to accumulation of DNA damage (Song *et al.*, 2018). Another study showed that loss of H2AX, a primary sensor of DNA damage, leads to EMT (Weyemi *et al.*, 2016), perhaps due to chromatin-mediated enhanced activity of EMT-TFs. Other works have pointed to a direct role of ZEB1 in the initial DNA damage response in tumor

cells either through stimulation of ATM expression (Zhang *et al.*, 2018) or stabilization of CHK1 (Zhang *et al.*, 2014), both resulting in enhanced homologous recombination. In contrast, a more recent study pointed to the role of ZEB1 in the recruitment of 53BP1, another sensor of DNA damage and a key factor in the choice of the repair pathway, to sites of double strand breaks to stimulate repair by non-homologous end joining (Genetta *et al.*, 2023).

In this work we directly explored the EMT-DDR connection by examining the impact on EMT of the inactivation of 53BP1. Our findings reveal that disabling 53BP1 leads to spontaneous EMT in a variety of tumor cells and that DDR inactivation does not impede further EMT reinforcement in response to exogenous damage. Moreover, 53BP1-abrogated cells showed increased expression of RAD51 in an EMT-TF-dependent manner and increased resistance to drugs. Mechanistically, we show that EMT-TFs bind to the RAD51 promoter and that, in response to DNA damage, PARP-dependent activation of ALC1 (CHD1L), a chromatin remodeler, allows the EMT-TF ZEB1 to access chromatin. Interestingly, inhibiting PARP activity with Olaparib or abolishing ALC1 both lead to a reversal of EMT-associated markers in DDR-deficient cells and sensitize them to other drugs.

RESULTS

DNA damage induces EMT biomarkers.

We have previously shown that spontaneous CIN in mortal Human Epithelial Kidney cells as well as long-term exposure of immortal HEK cells to DNA damage agents like etoposide lead to EMT (Castro-Vega *et al.*, 2013). To determine how soon after initial DNA damage EMT-related changes can be detected, we used the latter experimental system to precisely monitor in time responses such as cell morphology changes and gene expression of EMT- TFs, micro-RNAs (miRs) and other EMT-related markers. As early as 7 days after treatment initiation with low doses of etoposide (0.1 µM), epithelial cells displayed morphological changes, from cobble-like, tightly packed cells, to elongated, loosely packed fibroblastoid-like cells (Supplemental figure S1A). Of note, this treatment had no overt impact on growth rate of cells in the short term (not shown). Morphological changes were associated with a strong increase in the expression of all six EMT-TFs, as well as with an upregulation of mesenchymal markers including Vimentin, THBS1, MMP3, Serpine1 and FN1, along with a significant downregulation of epithelial markers such as E-cadherin (Supplemental Figure S1B). Most of these changes could also be detected at the protein level (Supplemental figure S1C) including some EMT-TFs. In addition, etoposide-treated cells displayed a significant down-regulation in the EMT-related miRs miR-200a, miR-200b, miR-200c (Supplemental Figure S1D). To ensure that this phenomenon is not exclusive to kidney-derived cell lines, MCF7 and HCT116 cancer cell lines, from breast and colon origin respectively, as well as the transformed prostate epithelial cell line PNT1A were treated with low doses of etoposide. As shown in Supplemental Figure S1E, all cell lines displayed a similar, albeit not identical, trend in expression changes affecting EMT-associated genes with downregulation of E-Cadherin in the case of MCF7 and HCT116, upregulation of some mesenchymal markers and of at least one EMT-TF in all cases. Altogether, these results demonstrate that DNA damage inflicted on epithelial cells rapidly induces an EMT response that can robustly be followed by cell morphology changes as well as changes in the expression of EMT-TFs and other EMT-associated markers.

DDR attenuation induces EMT in epithelial normal and neoplastic cells, that can be further stimulated by exogenous DNA damage.

To unravel the mechanistic link between DNA damage et EMT, we searched to block the DNA damage response pathway by inactivating key mediators such as 53BP1. 53BP1 is also a major contributor to repair pathway choice in response to double strand breaks (DSB) by protecting these breaks from resection thus favoring non-homologous end joining (NHEJ) over homologous recombination (HR) (Xu and Xu, 2020). We used the Cas9 (D10A)-based approach described by Chiang et al (Chiang *et al.*, 2016) to transform, sort and clone HEK-Early cells. Two 53BP1-KO clones were isolated with a complete inactivation of the locus (Figure 1A, Supplementary Figure 2A). Unexpectedly, 53BP1-KO cell clones spontaneously displayed a mesenchymal-like morphology (Figure 1B) and a higher expression of EMT-TFs along with the mesenchymal markers MMP3, FN1, Vimentin, THBS1, and Serpine1 (Figure 1C-D). Epithelial markers, on the other hand, showed diminished mRNA expression levels in 53BP1-KO cells (Figure 1C). Finally, miRNA(miR)-200 family members, which are key regulatory factors to maintain epithelial identity, were significantly downregulated in KO cells with respect to parental cells (Figure 1E), in agreement with the observed loss of epithelial characteristics. These results are highly reminiscent of those made by Weyemi et al, after elimination of H2AX, also a DDR sensor. To ascertain that the EMT-related phenotypes detected in 53BP1-KO clones were not due to off-target effects, we conducted rescue experiments by exogenously expressing 53BP1. 53BP1-KO cells were transfected with pcDNA3.1-53BP1 and kept in batch under antibiotic selection. Upon expression of exogenous 53BP1, the morphological features of 53BP1-KO cells displayed a remarkable shift from spindle-like, isolated mesenchymal cells towards packed, cobblestone, epithelial cells (Figure 1F). Further analyses confirmed this reversal as they revealed a significant downregulation of EMT-TFs and other mesenchymal markers such as MMP3, FN1, along with an increase in the expression of the epithelial markers E-cadherin, Lumican, and CDH3 (Figure 1G-H). The fact that 53BP1-KO cells were able to undergo MET when 53BP1 expression was restored underscores the fundamental plasticity that characterizes all EMT.

We noticed that restoring the expression of 53BP1 in these cells was also associated to a decrease in the spontaneous levels of DNA damage markers γH2AX, P-KAP1, and P-ATM (Figure 1I) further supporting the notion that eliminating 53BP1 may result in accumulation of spontaneous DNA lesions. To confirm that abrogation of a DDR component spontaneously leads to EMT, we targeted MDC1, another DNA damage sensor that also accumulates at DSBs (Lou *et al.*, 2003), for inactivation using the same Cas9 (D10A)-based approach. HEK-Early cells (53BP1 WT as well as 53BP1-KO cells) were transformed, sorted, and cloned as above and one clone KO for MDC1 was identified in each context (Supplementary figure S2A). In agreement with results described for 53BP1-KO cells, MDC1-KO and MDC1/53BP1-double KO HEK cells displayed cell morphology changes compatible with EMT (Supplementary figure S2B) as well as enhanced expression of EMT-TFs and mesenchymal markers along with significant downregulation of both epithelial markers (Supplementary figure S2C) and EMT-related miRs (Supplementary figure S2D).

All DDR-KO HEK-Early clones were further characterized for proliferation and migration capacities, features expected to be affected by the EMT process. We detected a significant decrease in the

proliferation rate of all KO clones in comparison with WT parental cells (Supplementary figure S2E), as previously shown for other cell lines undergoing EMT (Hugo *et al.*, 2017). Furthermore, all KO clones showed increased migration potential when compared to the parental cells, as evaluated in a wound healing assay (Figure 1J, Supplementary figure S2F).

Taken together, these results draw a strong link between DDR and EMT. They also support the notion that accumulation of endogenous damage (or exacerbation of DDR) – perhaps beyond a certain threshold- leads to EMT.

We verified that EMT in response to the elimination of a DDR component was a general feature in epithelial tumor cells from different tissues. We knocked out 53BP1 in the epithelial colon cancer cell line HCT116 (either P53 WT or P53-KO), in the epithelial breast cancer cell line MCF7, and in a prostate epithelial cell line immortalized by SV40, PNT1A (Supplementary figure S3A). Deletion of 53BP1 in all these cell lines induced both loss of epithelial cell morphology (Supplementary figure S3B) and increase in gene expression of EMT-TFs and mesenchymal-related markers (Figure 2A-E), while epithelial markers and the miR-200 family all appeared to be downregulated (Figure 2A-F). Like HEK-Early cells, all cell lines displayed higher migration potential than their WT counterparts (Figure 2G) (Supplementary figure S3C). Together, these results confirm that spontaneous EMT because of DDR perturbation is a general phenomenon in transformed epithelial cells, and that this EMT may occur independently of the p53 status.

The above results point to the possibility of a link between the levels of spontaneous DNA damage or DDR signaling found in a cell and the likelihood for that cell to undergo EMT. To determine whether further exposure to DNA damage could impact the DDR-related EMT phenotype already detected, we treated 53BP1-KO, and other knock-out cell clones, with etoposide 0.1 µM for 7 days and monitored the levels of EMT-related markers. As shown in Figure 3A (and Supplementary figure S4A), the mesenchymal aspect of KO cells was further reinforced. This phenomenon was coupled to a further increase in expression levels of EMT-TFs and other mesenchymal-related markers in 53BP1-KO (Figure 3B-C), as well as in MDC1-KO and MDC1/53BP1-KO (Supplementary figure S4B), while the expression of E-cadherin (albeit not that of Lumican) was further reduced. These results once again underscore the degree of plasticity of the EMT induced by the abrogation of one DDR component as well as the role played by DNA damage as a major trigger (or reinforcer) of EMT. They also formally establish that an intact DDR pathway is not absolutely required to escalate the EMT phenotypes in response to DNA damage.

EMT promotes DNA repair.

53BP1 rescue experiment supported the notion that in cells partially disabled for DDR, when the function is restored and EMT is suppressed, the levels of endogenous DNA damage diminished. To further explore the relationship between DNA damage and EMT, we targeted the EMT-TFs ZEB1 for downregulation using RNA interference in both HCT116 and PNT1A 53BP1-KO cells. ZEB1 downregulation led, as expected, to downregulation in the expression of mesenchymal markers such as Vimentin and MMP3, and to upregulation of epithelial markers such as E-cadherin and Lumican in all KO cell lines (Figure 4A-B). Strikingly, the downregulation of ZEB1 also led to an increase in the levels of

γH2AX in HCT116 53BP1-KO (Figure 4C), a phenomenon that we also observed when Slug was targeted for downregulation in the same cells (Supplementary figure 5A). This intriguing observation strongly suggested a role for EMT-TFs in the protection against the spontaneous accumulation of endogenous DNA damage. Another possibility is that EMT-TFs' activities somehow curb the intensity of the DDR. To confirm the potential role of EMT-TFs in DDR, we exogenously overexpressed TWIST1 in PNT1A cells, which display a relatively high level of spontaneous γH2AX. As expected, TWIST1 overexpression induced an increase of mesenchymal markers, such as Vimentin and a decrease in epithelial markers such as E-Cadherin (Figure 4D). Remarkably, PNT1A cells overexpressing TWIST1 also displayed a strong decrease in the level of γH2AX, supporting the conclusion that EMT reprogramming either improves DNA repair towards spontaneous DNA damage or restrain the levels of DDR (Figure 4D).

To assess a potential role of EMT more directly in DNA repair, we dynamically evaluated the efficiency of this repair in HCT116 cells, WT, or 53BP1-KO cells, depleted for ZEB1 and treated with etoposide for 24h. Cells were allowed to recover without the drug for 6 hours and the level of residual damage was determined by detecting γH2AX. As shown in Figure 4E, γH2AX levels decreased at 6h in control cells, while in both WT and 53BP1-KO ZEB1-depleted cells, the level of γH2AX increased instead. We confirmed these observations in MCF7 cells, WT, and 53BP1-KO, depleted or not for Slug (Supplementary figure S5B). In this case, cells were treated with etoposide and let to recover for 2 and 6 hours. Immunoblot analyses showed a rapid decrease in the levels of γH2AX in control cells, while in cells (WT or 53BP1-KO) depleted for Slug, this decrease took longer (Supplementary figure S5B). These experiments demonstrate for the first time a link between EMT-TFs and DNA repair efficiency, including tumor cells with intact DDR.

EMT supports a RAD51-dependent response.

To further establish a relationship between EMT-TFs and DNA repair, we examined the consequences of EMT-TFs downregulation on the levels of RAD51, a key actor of HR-mediated repair. Immunoblot analyses suggested that RAD51 levels are slightly increased in unperturbed 53BP1-KO cells with respect to parental cells (Figure 4F). Upon EMT-TF depletion, the levels of Rad51 decreased in both WT and 53BP1-KO HCT116 cells (Figure 4F), suggesting that these EMT-TFs control the expression of the Rad51 gene not only when cells undergo EMT but also in the epithelial state. The decrease on RAD51 expression upon knockdown of EMT-TFs and the concomitant increase in the levels of γH2AX strongly argue in favor of an accumulation of spontaneous DNA damage in these cells as opposed to a damage-independent exacerbation of DDR (Figure 4C, Supplementary figure S5A). These results were confirmed in immunofluorescence experiments, where we detected a significant decrease of spontaneous RAD51 foci upon depletion of EMT-TFs factors, both in WT and 53BP1-KO HCT116 cells, even though this depletion was associated with a significant increase in γH2AX foci (Figure 4G, Supplementary figure S5C). Finally, we examined the impact of EMT-TF depletion on drug resistance. While MCF7 53BP1-KO cells WT were more resistant to the drug than MCF7 WT (Supplementary figure S6A), both MCF7 53BP1-KO and WT cells depleted for ZEB1 or Slug were more sensitive than the control situation (Supplementary figure S6B-D). Together, these results indicate that the drug resistance characteristically

associated with EMT may be, at least in part, explained by the impact of EMT-TFs on RAD51 expression leading to more efficient DNA repair by HR.

EMT transcription factors bind to the RAD51 promoter.

Thus far, our results point to a positive role for EMT in the repair of both endogenous and exogenous DNA damage and suggest that 53BP1-KO EMT cells, which are expected to be deficient in NHEJ, rather repair damage using HR. To draw a direct link between EMT and activation of HR, we explored the possibility that EMT-TFs themselves could bind to the RAD51 promoter. Cut-and-run experiments were performed in HCT116 cells, unperturbed or depleted for ZEB1, using anti-ZEB1 antibodies (and anti-H3K27me3 antibodies as a positive control) followed by q-PCR that targeted two different regions of the RAD51 promoter (Figure 4H), as well as the promoter of vimentin, a known target for EMT-TFs as a positive control (Supplementary Figure S6E). We detected a >5-fold enrichment signal for ZEB1 on the RAD51 promoter, with respect to no antibody control, and this enrichment was completely abrogated in cells partially depleted for ZEB1 (Figure 4H). Similar results were obtained using an anti-Slug antibody in the same cells, unperturbed or depleted for Slug (Figure 4H). As expected, we also obtained enrichments for the Vimentin promoter with both anti-ZEB1 and anti-Slug antibodies (Supplementary Figure S6E). These results demonstrate that EMT-TFs promote DNA repair through direct stimulation of RAD51 transcription, also as confirmed by RT-qPCR after EMT-TF knock-downs (Supplemental Figure S6F).

The levels of expression of EMT-TFs and RAD51 are positively correlated in human tumors.

Finally, we sought to explore whether the connection we found between EMT-TFs and RAD51 in our experimental systems could be observed in a clinical setting. We carried out a comprehensive comparison of mRNA expression levels for EMT-TFs and RAD51 in both cancerous and normal tissues, leveraging publicly available RNAseq data from the TCGA consortium (http://gepia2.cancer-pku.cn/#index). Pooling the expression data for ZEB1, ZEB2, SNAI1, SNAI2 (Slug), TWIST1, and TWIST2 transcripts, we correlated their collective expression strength to the expression of RAD51 within the same tissue samples. Strikingly, our analysis revealed that among 34 paired correlations spanning 18 diverse cancer types, 32 exhibited a statistically significant positive correlation. Importantly, a substantial number of these correlations reached a high level of significance, as detailed in Table 1. The robust positive correlation observed in the majority of cases strongly suggests a clinically significant association between the expression of EMT-TFs and RAD51, shedding light on the intricate relationship between epithelial-to-mesenchymal transition and the DNA repair machinery in the context of cancer.

Chromatin accessibility for EMT-TFs during DNA damage hinges on the activities of PARP and ALC1.

Having shown that EMT-TFs factors promote repair by stimulating RAD51 transcription, we next explored how DNA damage may favor the transcriptional activity of EMT-TFs. Indeed, DNA damage induces increased DNA accessibility to repair factors and this accessibility depends on Poly (ADP-ribose) polymerase (PARP) activation and the subsequent activity of the PAR-binding chromatin remodeler CHD1L (ALC1)(Sellou *et al.*, 2016; Smith *et al.*, 2019). We wondered whether the same accessibility mechanisms were at play in the recruitment of EMT-TFs to promoters following DNA damage. To explore this possibility, we expressed a GFP-tagged ZEB1 version in U2OS cells, which were then subjected to

DNA damage induced by laser microirradiation under the microscope. As shown in Figure 5A, the fusion protein rapidly accumulates at the sites of damage. Strikingly, treatment of the cells with Olaparib, a PARP1/2 inhibitor in clinical use (Ledermann *et al.*, 2014) and known to block chromatin remodeling by ALC1 upon DNA damage (Sellou *et al.*, 2016), prevents the rapid recruitment of ZEB1 to the sites of damage. Interestingly, a C-terminally deleted version of ZEB1 (and therefore lacking the C-terminal zinc-finger cluster, see drawing in Figure 5A) showed less efficient chromatin binding upon DNA damage than the full-length protein (Figure 5A) strongly suggesting that, as shown for other proteins (Smith *et al.*, 2019), the recruitment of ZEB1 to chromatin in response to DNA damage is mediated through cognate sequences. Similar results were obtained in a cell context in which ALC1 had been abrogated (Figure 5B). These observations are compatible with the notion that chromatin relaxation mediated by ALC1 upon activation of PARP1 is a key step for EMT-TFs to access cognate sequences in response to DNA damage.

Inhibition of PARP reverses EMT and restores drug sensitivity.

We next tested the effect of Olaparib on the EMT features presented by cells with DDR deficiency. Treatment with Olaparib for only 3 days was sufficient to induce a strong reversal in the expression of EMT markers in HEK-early 53BP1-KO cells (Figure 5C). This rapid reversal of EMT markers by Olaparib was confirmed in PNT1A 53BP1-KO cells, which showed strong re-expression of E-cadherin and deep repression of both vimentin and fibronectin, as well as of most EMT-TFs (Figure 5D). Interestingly, Olaparib treatment also induced a reinforcement in E-cadherin expression and a further decrease of mesenchymal markers (including EMT-TFs) in DDR-proficient epithelial transformed cells (Figures 5C-D). In agreement with our observations demonstrating a mechanistic link between EMT-TFs and RAD51 expression to stimulate repair, PNT1A 53BP1-KO cells treated with Olaparib showed a decrease in the expression of RAD51 with an increase in γH2AX accumulation, all in association with a decrease in ZEB1 and TWIST1 proteins (Figure 5E).

To verify that the DDR-related EMT also requires ALC1, we deleted the gene in PNT1A 53BP1-KO cells and HCT116 53BP1-KO cells (Supplementary Figure 7A). As shown in Figure 5F (and Supplementary Figure S7B), abrogation of ALC1 led to re-expression of E-cadherin and to suppression of major EMT-TFs and mesenchymal markers in these cells. These observations are consistent with the idea that PARP-dependent chromatin relaxation is required for EMT-TFs activity to induce EMT and stimulate RAD51 expression and that inhibitors of PARP1/2 could be very efficient in reversing EMT hallmarks associated with a defective DDR.

BRCA-deficient cancer cells are exquisitely sensitive to PARP inhibitors (Evers *et al.*, 2008). We carried out cell survival tests for 53BP1-KO EMT cells in the presence of Olaparib, which revealed that these cells were also more sensitive to the inhibitor than 53BP1-proficient cells (Supplementary figure S8A-B). Interestingly, although 53BP1-deficient cells were more resistant than WT cells to drugs like Cisplatin or Taxol (Figure 6A-D), in agreement with their EMT status, the combination of Olaparib with these drugs restored their sensitivity (Figure 6A-D), also in agreement with the reversal of EMT hallmarks induced by Olaparib. These experiments demonstrate that inhibition of PARP can overturn the resistance to chemotherapeutic agents usually associated with EMT.

DISCUSSION

Here, we have shown again that transformed epithelial cells exposed to DNA damage undergo EMT. More importantly, we have provided evidence that this response depends on PARP/ALC1 activation, which then may allow EMT-TFs to access cognate promoters to initiate reprogramming. These results provide additional links between DNA damage and EMT-TFs, and thus EMT (Zhang *et al.*, 2014; Chiang *et al.*, 2016; Song *et al.*, 2018; Zhang *et al.*, 2018; Genetta *et al.*, 2023). However, for the first time, we also show in this work that RAD51, a key component of DNA repair by homologous recombination, is a major target of EMT-TFs thus allowing us to propose that stimulation of homologous recombination is a key aspect of the drug-resistance seen in tumor epithelial cells that undergo EMT.

Intriguingly, disabling 53BP1 or MDC1, key sensors that initiate DDR, and as such expected to participate in the EMT response, was spontaneously associated with an enduring EMT, which also depended on PARP/ALC1 activation. Our observations strongly suggest that the trigger of this reprogramming when DDR is abrogated appears to be the persistence of endogenous, unrepaired, DNA damage as suggested by the spontaneous increase in the levels of phosphorylation of DNA damage sensors such as ATM, KAP1 and H2AX. These results agree with a published work showing that abolishing H2AX, another DNA damage sensor, promotes EMT in HCT116 cells (Weyemi *et al.*, 2016). They also agree with studies showing that upon DNA damage ZEB1 binds to chromatin in a 53BP1-independent manner (Genetta *et al.*, 2023). Strikingly, 53BP1-KO, MDC1-KO and 53BP1/MDC1-DKO cells were still able to respond to additional exogenous DNA damage by reinforcing EMT-related traits, which could also be prevented by inhibiting PARP/ALC1 activation, thus underlying the extent of the plasticity acquired by cells under genomic stress.

How do DDR-deficient cells sense persistent DNA damage? Our experiments demonstrate that the PARP enzymatic activity is tightly involved in the sensing and transduction of the signal that leads to EMT. The role of PARP in EMT is not unprecedented since work by other groups already have pointed out that PARP inhibitors are able to prevent TGF-β-induced EMT in tumors cells (Pu *et al.*, 2014; Karicheva *et al.*, 2016; Schacke *et al.*, 2019), thus supporting the contention that PARP acts downstream from TGF-β activation. Given the role of PARP1 both as a DNA damage sensor and in the choice of DNA repair pathway, PARP activity appears to be the key component of the DDR-related EMT signaling pathway. Furthermore, inhibiting PARP1/2 or abrogating ALC1 were quite efficient in reversing already established DDR-related EMT phenotypes. Interestingly, this EMT reversion also encompasses a reversal of the enhanced resistance initially conferred by the EMT to clinically relevant chemotherapeutic drugs such as cis-platin and Taxol. Finally, transgenic animal models have suggested that, opposite to what has been described when PARP activity is inhibited, obliteration of the PARP1 gene leads to increased TGF-β and EMT during prostate tumorigenesis (Pu *et al.*, 2014). Potential explanations to this apparent conundrum include the fact that, although PARP1 is responsible for most of the ADP-ribosylation detected in cells, ADP-ribosylation in response to genotoxic stress is not totally abolished in PARP1-KO cells (Rank *et al.*, 2016). In fact, the presence of significant amounts of ADP-ribosylation in mouse embryonic fibroblasts from a PARP1-KO strain led to the discovery of PARP2 (Ame *et al.*, 1999), the other nuclear PARP enzyme whose activity in also enhanced in response to DNA damage (Chen *et al.*, 2018). Indeed,

simultaneous, and specific targeting of both PARP1 and PARP2 by Olaparib (Knezevic *et al.*, 2016) would explain why this inhibitor very efficiently prevents/reverses DNA damage related EMT phenotypes.

More generally, our results offer a sound mechanistic explanation helping to understand how EMT might be triggered during tumorigenesis. Indeed, DNA replication stress is omnipresent in cancer cells (Halazonetis *et al.*, 2008; Sotiriou and Halazonetis, 2019), which could provide a persistent source of endogenous DNA damage and as shown in this work, a trigger to trans-differentiation. Such replication stress is expected to occur early during tumorigenesis as oncogene activation leads to premature entry into S-phase and to activation of ectopic replication origins, thus creating replication/transcription conflicts ultimately leading to fork collapse and double strand breaks (Gorgoulis *et al.*, 2005). Indeed, signs of DNA damage response are often detected in precancerous lesions, followed by the detection of chromosome instability in early stages of tumor development (Gorgoulis *et al.*, 2005). Our data clearly point to the possibility that DNA damage-related EMT may occur as soon as the tumorigenic process initiates and that tumor cells may acquire metastatic properties at early stages of cancer progression. This hypothesis is supported by the demonstration of disseminated cancer cells (DCCs) in patients with breast cancer before any metastasis is detected (Hosseini *et al.*, 2016) and in transgenic mouse models of breast and pancreatic cancers as well as melanoma (Husemann *et al.*, 2008; Eyles *et al.*, 2010; Rhim *et al.*, 2012).

The present work also holds potential clinical implications. EMT has been previously directly connected to drug resistance (Shibue and Weinberg, 2017). Our findings open the possibility that the exposure of cancer cells to chemotherapeutic drugs has the potential to induce an EMT-like state in vivo. Our study shows that, at least in vitro, this DNA damage-related EMT response can not only be prevented but also reversed through the inhibition of PARP1/2 activity. Of note, PARP1/2 inhibitors like Olaparib have been approved for the treatment of BRCA mutated ovarian and breast cancers (Ledermann *et al.*, 2014) because HR-deficient tumor cells display an exquisite sensitivity to these inhibitors, which block the other major repair pathway NHEJ (Bryant *et al.*, 2005). This has led to the idea that cancer patients with mutations in other genes that participate in HR repair (such as ATM, ATR, BAP1, CDK12, CHEK2, FANCA, FANCC, FANCD2, FANCE, FANCF, PALB2, NBS1, WRN, RAD51C, RAD51D, MRE11A, CHEK1, BLM, and RAD51B) could also benefit from association treatments using PARP1/2 inhibitors (Boussios *et al.*, 2020). Here, we show that tumor cells deficient for 53BP1 (a major signaling molecule for NHEJ) also display increased sensitivity to PARP1/2 inhibitors. This apparently counterintuitive result may be explained by the fact that, as shown experimentally here and further supported by the significant co-expression of EMT-TFs and RAD51 in a variety of human cancers, EMT promotes DNA repair by stimulating RAD51 expression and the HR pathway. In the end, the possibility that PARP inhibitors perturb both major DNA repair pathways, particularly in cells that have undergone an EMT, might open new applications of these drugs in the clinic.

MATERIALS AND METHODS

Cell lines and cell culture

HA5-early cells are obtained from HEK (Human Epithelial Kidney) cells, as described by Castro-Vega et al. (Castro-Vega *et al.*, 2013). The PNT1A cell line was derived from human post-pubertal prostate normal epithelial cells transformed with SV40 (Degeorges *et al.*, 1995). HCT116 parental cells and

HCT116 P53-KO cells were obtained as gifts from Dr. Antonin Morillon and Dr. Franck Toledo, respectively. MCF7 and U2OS cells were obtained from ATCC. U2OS ALC1-KO cells were described previously (Sellou *et al.*, 2016). All cell lines were authenticated by STR analysis, tested for mycoplasma infection and cultured at 37 °C in a humidified atmosphere containing 5% CO2. HA5-early, PNT1A, and MCF7 parental and transfection-derived cell lines were cultured in Minimum Essential Medium-alpha 1X (MEM-α 1X) (Gibco; Life Technologies), supplemented with 10% (v/v) fetal bovine serum (FBS; Eurobio), 1% (v/v) MEM Non-essential Amino Acid Solution 100X (Gibco; Life technologies), and 1% (v/v) sodium pyruvate 100X (Gibco; Life technologies). HCT116 parental and transfected cells were cultured in McCoy's (5A)-modified (Gibco; Life Technologies) supplemented with 10% (v/v) fetal bovine serum. U2OS cells were cultured in DMEM (4.5 g/l glucose, Sigma) supplemented with 10% fetal bovine serum (Life Technologies), 2 mM glutamine (Sigma), 100 µg/ml penicillin and 100 U/ml streptomycin (Sigma).

All-in-one nickase plasmids

All-in-One-GFP and All-in-One-mCherry plasmids were purchased from Addgene (AIO-GFP #74119 and AIO-mCherry #74120). Their constructions have been described in (Chiang *et al.*, 2016).

Golden Gate assembly of CRISPR sgRNA cloning

53BP1 and MDC1 sgRNAs were inserted in an All-in-one nickase plasmids backbone as described by Chiang et al. (Chiang *et al.*, 2016) and the insertion and presence of both sgRNA sequences were verified by DNA Sanger sequencing in a single reaction using a primer: 5′-CTTGATGTACTGCCAAGTGGGC-3′. sgRNA sequences for 53BP1 and MDC1 are shown in Supplementary Table 1.

Transfection and transduction

To obtain 53BP1-KO, MDC1-KO, double 53BP1/MDC1-KO HA5-early cells, and 53BP1-KO PNT1A and MCF7 cells, parental cells were transfected with All-in-One nickase plasmids via electroporation using the amaxa-nucleofector® II according to the manufacturer's instructions (Thermofisher). 5-10 µg of the All-in-One plasmid were transfected into 106 cells. Cell Line NucleofectorTM Kit V (Catalog #: VCA-1003) (Lonza) was used for the transfection procedure according to the manufacturer's instructions. Q-001 program was applied to transfect. To obtain 53BP1-KO, HCT116 (including WT and P53-KO) cells were transfected using jetPRIME® (Reference number: 114-07) (Polyplus) according to the manufacturer's instructions. To obtain ALC1-KO cell lines, cells were transfected with the construct described in (Sellou *et al.*, 2016) using jetPRIME® (Reference number: 114-07) (Polyplus) according to the manufacturer's instructions. To obtain a knockdown of EMT-TFs in cells, HCT116, PNT1A, MCF7 parental, and 53BP1-KO cells were transfected with shZEB1 and shSlug (a kind gift from Pr. Alain Puisieux lab) and control shRNAs using jetPrime according to manufacturer's instructions. CRISPR knockouts were all verified by genotype screening and immunoblot analysis. shRNA Knockdown transfections followed by at least 3 weeks of selection by puromycin treatment. To obtain 53BP1 restored expressing cells, HA5-Early WT and 53BP1-KO cells were transduced with lentiviral particles packaged in 293T cells using the plasmid 53BP1.pcDNA3.1 (kind gift from Dr. Gaëlle Legube, University of Toulouse). The selection of transduced cells continued for three weeks under treatment with Hygromycin 75 µg/ml concentration. To obtain a

TWIST1 overexpressing clone from the PNT1A cell line, cells were transfected with Twist (TWIST1) (NM_000474) Human Tagged ORF Clone (Origene). Transfected cells underwent 3 weeks selection procedure with Neomycin (400 µg/ml). For transient expression of GFP-tagged ZEB1, U2OS cells were transfected 12–24 h after seeding into eight-well Imaging Chamber CG (Zell-Kontakt) with XtremeGENE HP (Sigma) according to the manufacturer's instructions and incubated for 48 h before imaging.

Fluorescence-activated cell sorting (FACS)

72 hours after transfection, cells were trypsinized, washed with PBS, resuspended in PBS (supplemented with 2% FBS) and filtered through cell strained capped 5 ml falcon (STEM CELL). Cells were individually sorted, either based on GFP, mCherry, or mCherry+EGFP markers into TPP tissue culture test plate-96 (SIGMA-ALDRICH) at a single-cell-per-well density for clonal expansion. Subsequently, all viable clones passed through the genotyping screening and Immunoblot analysis.

CRISPR KO clone selection

Single-cell sorting following each transfection was continued by the propagation of clones in the P96-well plate and passage into the P24-well plate, then into the P6-well plate. Cell pellets were collected after washing and trypsinization for DNA and protein analysis. Clones were verified by immunoblotting after initial genotype screening and DNA sequencing indicating rearrangement of the relevant locus. When possible, at least two clones were randomly selected for this study.

Genomic DNA extraction

For genotype screening, genomic DNA was extracted from clones in a 96-well plate format. To extract DNA, cells were washed with 200 µl PBS and incubated in 50 µl Lysis buffer (10 mM Tris pH 7.5, 10 mM EDTA, 10 mM NaCl, 0.5 % sarcosyl) overnight at 55°C. DNA precipitated and attached to the surface by adding 100 µl chilled EtOH + 75mM NaCl and incubated for at least 30 minutes at room temperature. The lysates were removed by traversing the plate. DNA was washed by incubation with 150 µl 70% EtOH. EtOH was removed and DNA was solved in 30 µl DEPC-treated water. For DNA sequencing, genomic DNA was extracted using the Qiamp DNA mini kit (QIAGEN) according to the manufacturer's instructions.

PCR and Genotype screening

All PCRs in this study were performed with a Promega PCR master kit according to the manufacturer's instructions. PCR products were separated on the agarose gels and analyzed by the Geldoc XR+ system (Biorad). PCR products were sequenced by using gene-specific primers. A list of the PCR primers used for genotypic screening or DNA sequencing is shown in Supplementary Table S2.

Immunoblotting

Proteins were extracted with lysis buffer (1% Triton, and 50 mM Tris-HCl, pH 8.0, 300 µM NaCl, 5 mM EDTA). Protein concentrations were determined with a BMG Labtech FluoStar Optima Plate Reader at 560 nm. Samples were then heated to 95 °C for 5 minutes following the addition of loading dye. Proteins are separated by NuPAGE™ 4-12% Bis-Tris precast protein gels (Thermo Fisher Scientific) and then transferred to nitrocellulose membrane (GE Healthcare). To confirm homogeneous loading and transferring, membranes were stained with Ponceau S. Then Ponceau S-stained membranes were

washed with PBS tween followed by 1-hour incubation with blocking solution 5% BSA-PBS tween or 5% milk-PBS tween. Then the membrane was incubated overnight with primary antibodies diluted in a blocking solution. The primary antibody was washed with PBS tween and the membrane was incubated with a specific secondary antibody diluted in a blocking solution. Antibodies used in this study are listed in Supplementary Table S3.

Quantitative RT-PCR

RNeasy mini kit (Qiagen) was used to extract RNA from cells, according to the manufacturer's instructions. RNA was resuspended in DEPC-treated water. Synthesis of cDNA with Superscript III reverse transcriptase (Invitrogen) was primed with oligo (dT). Primer sequences are shown in Supplementary Table S4. Analyses were carried out using Promega PCR master mix (Promega) on an LC-480 Real-Time PCR system (Roche). Amounts of target mRNA were normalized to an endogenous housekeeping gene (β-actin) and calculated as fold change over control or parental cell lines.

To perform QRT-PCR analysis for miRNAs, the miRNeasy kit was used to extract total RNA and microRNAs. Then miRCURY LNA™ Universal RT microRNA cDNA Synthesis Kit (ThermoFischer) was used for RT PCR according to the manufacturer's instructions. miRCURY LNA SYBR® Green PCR Kit (Qiagen) was used for QRT-PCR according to manufacturer instructions and as described in (5).

Proliferation assays

Cells were plated in a cell culture P12 plate at a density of 10,000 cells in triplicates. Every 24 hours wells were trypsinized and resuspended in media. 200µl of cell suspension was diluted in 10ml of isotone solution and counted by Beckman Coulter Z2 cell/particle counter. The last counting is performed 96 hours after cell plating.

Wound healing or migration assays

Cells were plated and grown to full confluence in 6-well plates. Pipette tips were used to create scratches in the monolayers. Pictures were taken by an inverted light microscope in T0 (beginning of the experiment) and T1, variable time depending on the cell line (between 6 and 24 hours) after wounding.

Cell survival assays

10,000 Cells per well were plated and grown for 24 hours in 96-well plates. Cells were treated in serial diluted concentrations of each drug indicated in the text. Treatments lasted 96 hours. After 4 days, the density of cells in each well was quantified using Methylene Blue staining. In the first step, cells (wells) were washed with PBS 1X. Then 100 µl absolute methanol was added to each well and the plate was incubated for 1 hour at room temperature. Then the wells were let dry and 100 µl methylene blue solution (concentration 1gr/L) was added to each well and followed by 1-hour incubation at room temperature. Following the staining step, wells were rinsed with water 2 times and then let the wells dry. The washing step was followed by solubilization by adding 200 µl HCL (0.1N) in each well and incubation at 60°C for 30 minutes. In the last step, the O.D of each well was measured at 630 nm using a BMG FLUOstar OPTIMA plate reader.

Drug treatments

For each treatment experiment, cells were plated at an appropriate density 24 hours before treatment. The dosages indicated in the text for each treatment were selected according to the cell lines specific IC50 values and the duration of the treatment period. Each drug treatment was refreshed every 48-72 hours according to the manufacturer's indications. Treatment was removed and followed by washing with PBS 1X to collect the pellet to perform QRT-PCR and/or Immunoblotting. The following drugs were used in this study: Etoposide (S1225) (Selleckchem), Olaparib (AZD2281) (Selleckchem), Cisplatine (Mylan, 100mg/100ml) and Taxol (Paclitaxel) (S1150) (Selleckchem).

Etoposide treatment recovery assays

100K Cells per well were plated and grown for 24 hours in 6-well plates. Cells were treated with the indicated Etoposide concentrations and incubated for the mentioned time. Following the removal of the Etoposide treatment, wells were washed with PBS 1X and collected by trypsinization after the indicated time following the removal of treatment.

IF cell-staining and microscopy-based screening

Cells were washed with PBS containing 0.1% Tween-20 (PBST) and fixed for 15 min in PBS containing 2% paraformaldehyde. After fixation, cells were permeabilized in PBS containing 0.2–0.5% Triton X-100 for 10–15 minutes and blocked with blocking buffer (PBST with 5% (w/v) BSA) for 30 minutes. After three washes with PBST, immunostaining was performed with the indicated primary antibodies (Supplementary Table S3) diluted in the blocking buffer for 1 hour at room temperature followed by three washes with PBST. Cells were then stained with the appropriate secondary antibodies for 1h at room temperature diluted in blocking buffer followed by another three washes with PBST. Cells were counterstained with DAPI (1 µg/ml) and mounted using Vectashield (Vector Labs). Images were acquired with a Zeiss Axio Imager Fluorescence Microscope. Images were analyzed using Image J.

Cleavage under targets and release using nuclease (CUT&RUN)

CUT&RUN experiment according to the protocol described by Skene et al (Skene *et al.*, 2018). ZEB1 (Origene, # TA802298) and Slug (Origene, # OTI1A6) antibodies were used. As a positive control α-H3K27me3 rabbit monoclonal antibody (Cell Signaling Technology, # 9733). As a negative control, a mouse IgG antibody was used. DNA precipitation is followed by DNA purification according to the same protocol. QPCR was done for the Rad51 promoter using three sets of primers (see Supplementary Table 4) and data normalized to Alu as a reference and then made ratio to positive control.

Fluorescence imaging, laser micro-irradiation, and ZEB1 recruitment kinetics to DNA lesions

Before live cell imaging combined with laser irradiation, U2OS cells were presensitized with 0.3 µg/ml Hoechst 33342 for 1 h at 37◦C. Then, the growth medium was replaced with a CO2-independent imaging medium (Phenol Red-free Leibovitz's L-15 medium (Life Technologies) supplemented with 20% fetal bovine serum, 100 µg/ml penicillin and 100 U/ml streptomycin). For PARP inhibition, cells were treated with 30 µM Olaparib (Euromedex) for 30 min before imaging. Live-cell imaging experiments combined with laser irradiation were performed on a Ti-E inverted microscope (Nikon) equipped with a CSU-X1

spinning disk head (Yokogawa). The cells were imaged with a Plan APO 60×/1.4 NA oil-immersion objective lens and an sCMOS ORCA Flash 4.0 camera. The fluorescence of EGFP was excited at 490 and detected with a bandpass filter at 500-550 nm. Laser microirradiation was performed along a 16 µm-line through the nucleus using a single-point scanning head (iLas2 from Roper Scientific) coupled to the epifluorescence backboard of the microscope. To ensure reproducibility, laser power at 405 nm was measured at the beginning of each experiment and set to 125 µW at the sample level. Cells were maintained at 37◦C with a heating chamber in the absence of CO2. These experiments were completed with unsynchronized cells. The recruitment kinetics were quantified with FIJI (https://fiji.sc/). The image sequences were first registered using the MultiStackReg plugin (Thevenaz *et al.*, 1998), and then regions of interest were delineated manually to measure the mean fluorescence intensity in the damaged region (Id), in the whole nucleus (In), and a background region outside of the cell (Ibg). Protein accumulation at sites of damage (Ad) was then calculated as:

$$A_d = \frac{I_d - I_{bg}}{I_n - I_{bg}}$$

The intensity within the micro-irradiated area was then normalized to the intensity before damage induction.

Statistical analysis

Data was obtained from a minimum of 3 independent experiments. For PCR, each experiment was done in triplicate. In bar graphs and dose-response curves, comparisons between control and test samples were performed using either the two-way ANOVA test (Dunnett's multiple comparisons test), Student's t-test, or multiple t-tests. All statistical tests used a two-tailed α = 0.05 level of significance and were performed using GraphPad Prism (GraphPad Software). For all studies, curves show pooled data with error bars representing SEM obtained from at least three independent experiments. For cytotoxic curves, significance is indicated in the graphs as follows: *, P < 0.05; **, P < 0.01; ***, P < 0.001; ****, P < 0.0001.

Data and materials availability: All data (original pictures or excel files) and materials used in the analyses are available. All data are available in the main text or the supplementary materials.

Supplemental data: Supplementary Data are available at MBoC Online.

Acknowledgments: Authors are grateful to all Londono-Vallejo Laboratory members for stimulating discussions. We thank the A. Morillon, F. Toledo, G. Legube, A. Puisieux, S. Jackson and U. Weyemi laboratories for biological material. Work in the Londono-Vallejo laboratory has been supported by grants from the Fondation ARC (to ALV); the French Institut National du Cancer (INCa) (to ALV); the INCa-Ligue-ARC PAIR prostate cancer program (to ALV) and the Institut Curie post-doctoral program (to FR).

Competing Interest Statement: Authors declare that they have no competing interests.

REFERENCES

Ame, J.C., Rolli, V., Schreiber, V., Niedergang, C., Apiou, F., Decker, P., Muller, S., Hoger, T., Menissier-de Murcia, J., and de Murcia, G. (1999). PARP-2, A novel mammalian DNA damage-dependent poly(ADP-ribose) polymerase. J Biol Chem *274*, 17860-17868.

Bakhoum, S.F., Ngo, B., Laughney, A.M., Cavallo, J.A., Murphy, C.J., Ly, P., Shah, P., Sriram, R.K., Watkins, T.B.K., Taunk, N.K., Duran, M., Pauli, C., Shaw, C., Chadalavada, K., Rajasekhar, V.K., Genovese, G., Venkatesan, S., Birkbak, N.J., McGranahan, N., Lundquist, M., LaPlant, Q., Healey, J.H., Elemento, O., Chung, C.H., Lee, N.Y., Imielenski, M., Nanjangud, G., Pe'er, D., Cleveland, D.W., Powell, S.N., Lammerding, J., Swanton, C., and Cantley, L.C. (2018). Chromosomal instability drives metastasis through a cytosolic DNA response. Nature *553*, 467-472.

Boussios, S., Abson, C., Moschetta, M., Rassy, E., Karathanasi, A., Bhat, T., Ghumman, F., Sheriff, M., and Pavlidis, N. (2020). Poly (ADP-Ribose) Polymerase Inhibitors: Talazoparib in Ovarian Cancer and Beyond. Drugs R D *20*, 55-73.

Bryant, H.E., Schultz, N., Thomas, H.D., Parker, K.M., Flower, D., Lopez, E., Kyle, S., Meuth, M., Curtin, N.J., and Helleday, T. (2005). Specific killing of BRCA2-deficient tumours with inhibitors of poly(ADP-ribose) polymerase. Nature *434*, 913-917.

Castro-Vega, L.J., Jouravleva, K., Liu, W.Y., Martinez, C., Gestraud, P., Hupe, P., Servant, N., Albaud, B., Gentien, D., Gad, S., Richard, S., Bacchetti, S., and Londono-Vallejo, A. (2013). Telomere crisis in kidney epithelial cells promotes the acquisition of a microRNA signature retrieved in aggressive renal cell carcinomas. Carcinogenesis *34*, 1173-1180.

Castro-Vega, L.J., Jouravleva, K., Ortiz-Montero, P., Liu, W.Y., Galeano, J.L., Romero, M., Popova, T., Bacchetti, S., Vernot, J.P., and Londono-Vallejo, A. (2015). The senescent microenvironment promotes the emergence of heterogeneous cancer stem-like cells. Carcinogenesis *36*, 1180-1192.

Chen, Q., Kassab, M.A., Dantzer, F., and Yu, X. (2018). PARP2 mediates branched poly ADP-ribosylation in response to DNA damage. Nat Commun *9*, 3233.

Chiang, T.W., le Sage, C., Larrieu, D., Demir, M., and Jackson, S.P. (2016). CRISPR-Cas9(D10A) nickase-based genotypic and phenotypic screening to enhance genome editing. Sci Rep *6*, 24356.

Degeorges, A., Hoffschir, F., Cussenot, O., Gauville, C., Le Duc, A., Dutrillaux, B., and Calvo, F. (1995). Recurrent cytogenetic alterations of prostate carcinoma and amplification of c-myc or epidermal growth factor receptor in subclones of immortalized PNT1 human prostate epithelial cell line. Int J Cancer *62*, 724-731.

Derynck, R., and Weinberg, R.A. (2019). EMT and Cancer: More Than Meets the Eye. Dev Cell *49*, 313-316.

Evers, B., Drost, R., Schut, E., de Bruin, M., van der Burg, E., Derksen, P.W., Holstege, H., Liu, X., van Drunen, E., Beverloo, H.B., Smith, G.C., Martin, N.M., Lau, A., O'Connor, M.J., and Jonkers, J. (2008). Selective inhibition of BRCA2-deficient mammary tumor cell growth by AZD2281 and cisplatin. Clin Cancer Res *14*, 3916-3925.

Eyles, J., Puaux, A.L., Wang, X., Toh, B., Prakash, C., Hong, M., Tan, T.G., Zheng, L., Ong, L.C., Jin, Y., Kato, M., Prevost-Blondel, A., Chow, P., Yang, H., and Abastado, J.P. (2010). Tumor cells disseminate early, but immunosurveillance limits metastatic outgrowth, in a mouse model of melanoma. J Clin Invest *120*, 2030-2039.

Genetta, T.L., Hurwitz, J.C., Clark, E.A., Herold, B.T., Khalil, S., Abbas, T., and Larner, J.M. (2023). ZEB1 promotes non-homologous end joining double-strand break repair. Nucleic Acids Res *51*, 9863-9879.

Gorgoulis, V.G., Vassiliou, L.V., Karakaidos, P., Zacharatos, P., Kotsinas, A., Liloglou, T., Venere, M., Ditullio, R.A., Jr., Kastrinakis, N.G., Levy, B., Kletsas, D., Yoneta, A., Herlyn, M.,

Kittas, C., and Halazonetis, T.D. (2005). Activation of the DNA damage checkpoint and genomic instability in human precancerous lesions. Nature *434*, 907-913.
Halazonetis, T.D., Gorgoulis, V.G., and Bartek, J. (2008). An oncogene-induced DNA damage model for cancer development. Science *319*, 1352-1355.
Harper, E.I., Sheedy, E.F., and Stack, M.S. (2018). With Great Age Comes Great Metastatic Ability: Ovarian Cancer and the Appeal of the Aging Peritoneal Microenvironment. Cancers (Basel) *10*.
Hosseini, H., Obradovic, M.M.S., Hoffmann, M., Harper, K.L., Sosa, M.S., Werner-Klein, M., Nanduri, L.K., Werno, C., Ehrl, C., Maneck, M., Patwary, N., Haunschild, G., Guzvic, M., Reimelt, C., Grauvogl, M., Eichner, N., Weber, F., Hartkopf, A.D., Taran, F.A., Brucker, S.Y., Fehm, T., Rack, B., Buchholz, S., Spang, R., Meister, G., Aguirre-Ghiso, J.A., and Klein, C.A. (2016). Early dissemination seeds metastasis in breast cancer. Nature *540*, 552-558.
Hugo, H.J., Gunasinghe, N., Hollier, B.G., Tanaka, T., Blick, T., Toh, A., Hill, P., Gilles, C., Waltham, M., and Thompson, E.W. (2017). Epithelial requirement for in vitro proliferation and xenograft growth and metastasis of MDA-MB-468 human breast cancer cells: oncogenic rather than tumor-suppressive role of E-cadherin. Breast Cancer Res *19*, 86.
Husemann, Y., Geigl, J.B., Schubert, F., Musiani, P., Meyer, M., Burghart, E., Forni, G., Eils, R., Fehm, T., Riethmuller, G., and Klein, C.A. (2008). Systemic spread is an early step in breast cancer. Cancer Cell *13*, 58-68.
Karicheva, O., Rodriguez-Vargas, J.M., Wadier, N., Martin-Hernandez, K., Vauchelles, R., Magroun, N., Tissier, A., Schreiber, V., and Dantzer, F. (2016). PARP3 controls TGFbeta and ROS driven epithelial-to-mesenchymal transition and stemness by stimulating a TG2-Snail-E-cadherin axis. Oncotarget *7*, 64109-64123.
Kass, E.M., Moynahan, M.E., and Jasin, M. (2016). When Genome Maintenance Goes Badly Awry. Mol Cell *62*, 777-787.
Knezevic, C.E., Wright, G., Rix, L.L.R., Kim, W., Kuenzi, B.M., Luo, Y., Watters, J.M., Koomen, J.M., Haura, E.B., Monteiro, A.N., Radu, C., Lawrence, H.R., and Rix, U. (2016). Proteome-wide Profiling of Clinical PARP Inhibitors Reveals Compound-Specific Secondary Targets. Cell Chem Biol *23*, 1490-1503.
Ledermann, J., Harter, P., Gourley, C., Friedlander, M., Vergote, I., Rustin, G., Scott, C.L., Meier, W., Shapira-Frommer, R., Safra, T., Matei, D., Fielding, A., Spencer, S., Dougherty, B., Orr, M., Hodgson, D., Barrett, J.C., and Matulonis, U. (2014). Olaparib maintenance therapy in patients with platinum-sensitive relapsed serous ovarian cancer: a preplanned retrospective analysis of outcomes by BRCA status in a randomised phase 2 trial. Lancet Oncol *15*, 852-861.
Lou, Z., Minter-Dykhouse, K., Wu, X., and Chen, J. (2003). MDC1 is coupled to activated CHK2 in mammalian DNA damage response pathways. Nature *421*, 957-961.
Lynch, H.T., Shaw, T.G., and Lynch, J.F. (2004). Inherited predisposition to cancer: a historical overview. Am J Med Genet C Semin Med Genet *129C*, 5-22.
Maser, R.S., and DePinho, R.A. (2002). Connecting chromosomes, crisis, and cancer. Science *297*, 565-569.
Nowak, M.A., Komarova, N.L., Sengupta, A., Jallepalli, P.V., Shih Ie, M., Vogelstein, B., and Lengauer, C. (2002). The role of chromosomal instability in tumor initiation. Proc Natl Acad Sci U S A *99*, 16226-16231.
Ortiz-Montero, P., Londono-Vallejo, A., and Vernot, J.P. (2017). Senescence-associated IL-6 and IL-8 cytokines induce a self- and cross-reinforced senescence/inflammatory milieu strengthening tumorigenic capabilities in the MCF-7 breast cancer cell line. Cell Commun Signal *15*, 17.
Pastushenko, I., and Blanpain, C. (2019). EMT Transition States during Tumor Progression and Metastasis. Trends Cell Biol *29*, 212-226.

Pu, H., Horbinski, C., Hensley, P.J., Matuszak, E.A., Atkinson, T., and Kyprianou, N. (2014). PARP-1 regulates epithelial-mesenchymal transition (EMT) in prostate tumorigenesis. Carcinogenesis *35*, 2592-2601.
Puisieux, A., Brabletz, T., and Caramel, J. (2014). Oncogenic roles of EMT-inducing transcription factors. Nat Cell Biol *16*, 488-494.
Rajagopalan, H., and Lengauer, C. (2004). CIN-ful cancers. Cancer Chemother Pharmacol *54 Suppl 1*, S65-68.
Rank, L., Veith, S., Gwosch, E.C., Demgenski, J., Ganz, M., Jongmans, M.C., Vogel, C., Fischbach, A., Buerger, S., Fischer, J.M., Zubel, T., Stier, A., Renner, C., Schmalz, M., Beneke, S., Groettrup, M., Kuiper, R.P., Burkle, A., Ferrando-May, E., and Mangerich, A. (2016). Analyzing structure-function relationships of artificial and cancer-associated PARP1 variants by reconstituting TALEN-generated HeLa PARP1 knock-out cells. Nucleic Acids Res *44*, 10386-10405.
Rhim, A.D., Mirek, E.T., Aiello, N.M., Maitra, A., Bailey, J.M., McAllister, F., Reichert, M., Beatty, G.L., Rustgi, A.K., Vonderheide, R.H., Leach, S.D., and Stanger, B.Z. (2012). EMT and dissemination precede pancreatic tumor formation. Cell *148*, 349-361.
Romero-Laorden, N., and Castro, E. (2017). Inherited mutations in DNA repair genes and cancer risk. Curr Probl Cancer *41*, 251-264.
Schacke, M., Kumar, J., Colwell, N., Hermanson, K., Folle, G.A., Nechaev, S., Dhasarathy, A., and Lafon-Hughes, L. (2019). PARP-1/2 Inhibitor Olaparib Prevents or Partially Reverts EMT Induced by TGF-beta in NMuMG Cells. Int J Mol Sci *20*.
Sellou, H., Lebeaupin, T., Chapuis, C., Smith, R., Hegele, A., Singh, H.R., Kozlowski, M., Bultmann, S., Ladurner, A.G., Timinszky, G., and Huet, S. (2016). The poly(ADP-ribose)-dependent chromatin remodeler Alc1 induces local chromatin relaxation upon DNA damage. Mol Biol Cell *27*, 3791-3799.
Shibue, T., and Weinberg, R.A. (2017). EMT, CSCs, and drug resistance: the mechanistic link and clinical implications. Nat Rev Clin Oncol *14*, 611-629.
Shih, I.M., Zhou, W., Goodman, S.N., Lengauer, C., Kinzler, K.W., and Vogelstein, B. (2001). Evidence that genetic instability occurs at an early stage of colorectal tumorigenesis. Cancer Res *61*, 818-822.
Skene, P.J., Henikoff, J.G., and Henikoff, S. (2018). Targeted in situ genome-wide profiling with high efficiency for low cell numbers. Nat Protoc *13*, 1006-1019.
Smith, R., Lebeaupin, T., Juhasz, S., Chapuis, C., D'Augustin, O., Dutertre, S., Burkovics, P., Biertumpfel, C., Timinszky, G., and Huet, S. (2019). Poly(ADP-ribose)-dependent chromatin unfolding facilitates the association of DNA-binding proteins with DNA at sites of damage. Nucleic Acids Res *47*, 11250-11267.
Song, N., Jing, W., Li, C., Bai, M., Cheng, Y., Li, H., Hou, K., Li, Y., Wang, K., Li, Z., Liu, Y., Qu, X., and Che, X. (2018). ZEB1 inhibition sensitizes cells to the ATR inhibitor VE-821 by abrogating epithelial-mesenchymal transition and enhancing DNA damage. Cell Cycle *17*, 595-604.
Sotiriou, S.K., and Halazonetis, T.D. (2019). Remodeling Collapsed DNA Replication Forks for Cancer Development. Cancer Res *79*, 1297-1298.
Stemmler, M.P., Eccles, R.L., Brabletz, S., and Brabletz, T. (2019). Non-redundant functions of EMT transcription factors. Nat Cell Biol *21*, 102-112.
Taylor, B.S., Schultz, N., Hieronymus, H., Gopalan, A., Xiao, Y., Carver, B.S., Arora, V.K., Kaushik, P., Cerami, E., Reva, B., Antipin, Y., Mitsiades, N., Landers, T., Dolgalev, I., Major, J.E., Wilson, M., Socci, N.D., Lash, A.E., Heguy, A., Eastham, J.A., Scher, H.I., Reuter, V.E., Scardino, P.T., Sander, C., Sawyers, C.L., and Gerald, W.L. (2010). Integrative genomic profiling of human prostate cancer. Cancer Cell *18*, 11-22.

Thevenaz, P., Ruttimann, U.E., and Unser, M. (1998). A pyramid approach to subpixel registration based on intensity. IEEE Trans Image Process *7*, 27-41.
Watanabe, T., Kobunai, T., Yamamoto, Y., Matsuda, K., Ishihara, S., Nozawa, K., Yamada, H., Hayama, T., Inoue, E., Tamura, J., Iinuma, H., Akiyoshi, T., and Muto, T. (2012). Chromosomal instability (CIN) phenotype, CIN high or CIN low, predicts survival for colorectal cancer. J Clin Oncol *30*, 2256-2264.
Weyemi, U., Redon, C.E., Choudhuri, R., Aziz, T., Maeda, D., Boufraqech, M., Parekh, P.R., Sethi, T.K., Kasoji, M., Abrams, N., Merchant, A., Rajapakse, V.N., and Bonner, W.M. (2016). The histone variant H2A.X is a regulator of the epithelial-mesenchymal transition. Nat Commun *7*, 10711.
Wolters, S., and Schumacher, B. (2013). Genome maintenance and transcription integrity in aging and disease. Front Genet *4*, 19.
Xu, Y., and Xu, D. (2020). Repair pathway choice for double-strand breaks. Essays Biochem.
Zhang, P., Wei, Y., Wang, L., Debeb, B.G., Yuan, Y., Zhang, J., Yuan, J., Wang, M., Chen, D., Sun, Y., Woodward, W.A., Liu, Y., Dean, D.C., Liang, H., Hu, Y., Ang, K.K., Hung, M.C., Chen, J., and Ma, L. (2014). ATM-mediated stabilization of ZEB1 promotes DNA damage response and radioresistance through CHK1. Nat Cell Biol *16*, 864-875.
Zhang, X., Zhang, Z., Zhang, Q., Zhang, Q., Sun, P., Xiang, R., Ren, G., and Yang, S. (2018). ZEB1 confers chemotherapeutic resistance to breast cancer by activating ATM. Cell Death Dis *9*, 57.

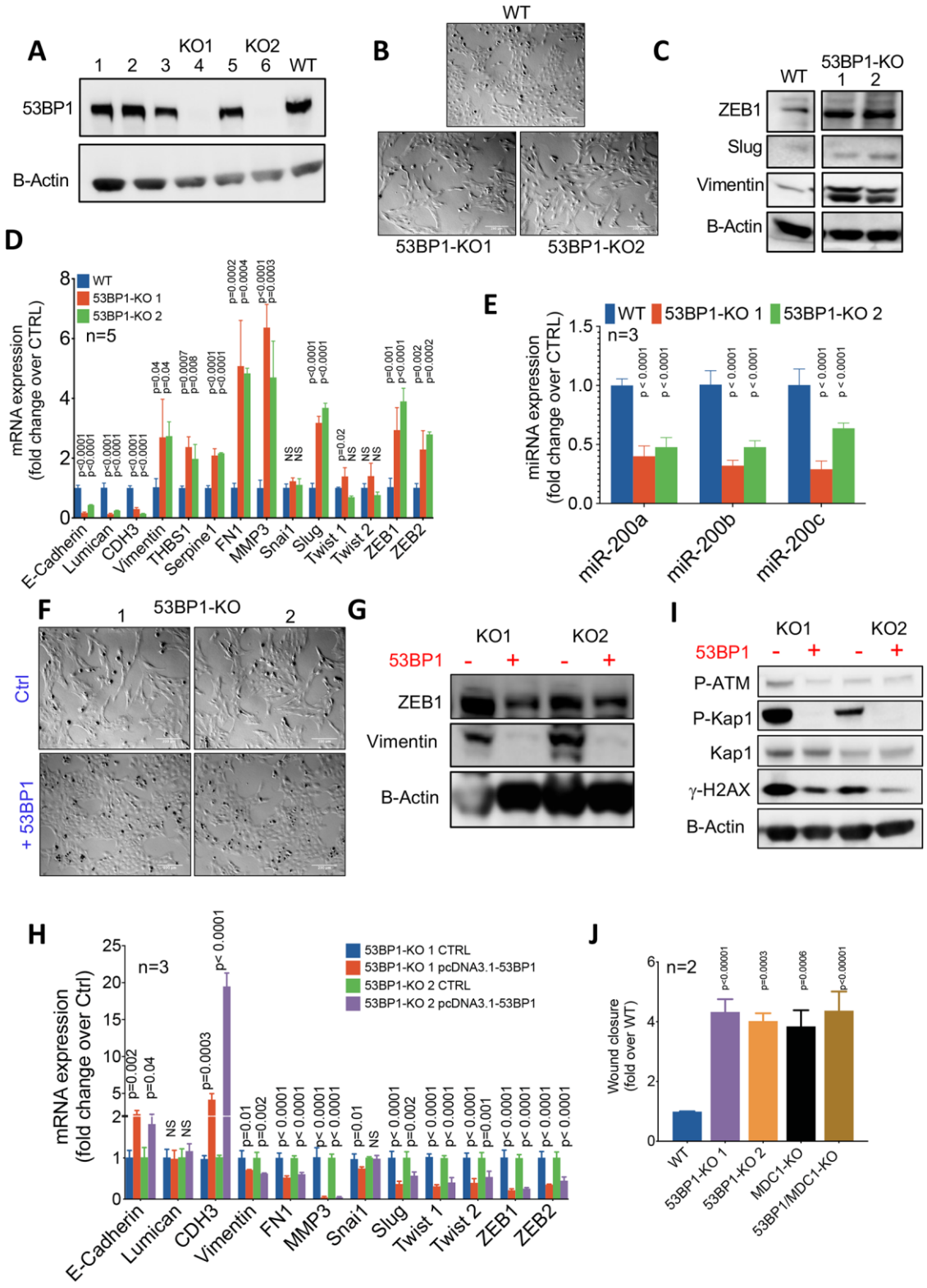

Figure 1. Disabling the DNA Damage Response induces EMT.

A. Identification by western blot of CRISPR-Cas9 transfected HEK-Early clones with full KO for 53BP1 (KO1 and KO2). **B.** Cell morphology aspect of KO clones compared with the parental cell line (WT). Scale bar=200µm. **C.** Western blot analyses for EMT-related markers in 53BP1-KO clones. **D.** Relative mRNA level of expression for epithelial and EMT markers in 53BP1-KO

clones compared to the parental cell line (WT). P-values from comparisons with control (Dunnett's multiple comparisons test) are indicated. NS: non-significant. **E.** Relative expression level of three members of the miR-200 family upon deletion of 53BP1. P-values from comparisons with control (Dunnett's multiple comparisons test) are indicated. **F.** Cell morphology aspect of 53BP1-KO clones before and after forced expression of exogenous 53BP1 (+53PB1). Scale bar=200µm. **G.** Western blot analyses showing the impact, on EMT-related markers, of 53BP1 re-expression in 53BP1-KO clones. **H.** Relative mRNA level of expression of epithelial and EMT markers in 53BP1-KO clones upon forced expression of exogenous 53BP1. P-values from paired comparisons (Dunnett's multiple comparisons test) with cells transfected with a control (CTRL) plasmid are indicated. NS: non-significant. **I.** Western blot analyses showing the evolution of DNA damage markers P-ATM, P-KAP1 and γH2AX in 53BP1-KO clones upon forced expression of exogenous 53BP1. **J.** Quantification of wound healing assays carried out with 53BP1-KO, MDC1-KO and 53BP1/MDC1-DKO cells. Represented are means of relative wound closures by KO clones after 20h in comparison to the parental cell line (WT). Original mages are presented in Supplementary Figure S3G. P-values correspond to pairwise comparisons (Kruskal-Wallis test) with the parental cell line (WT).

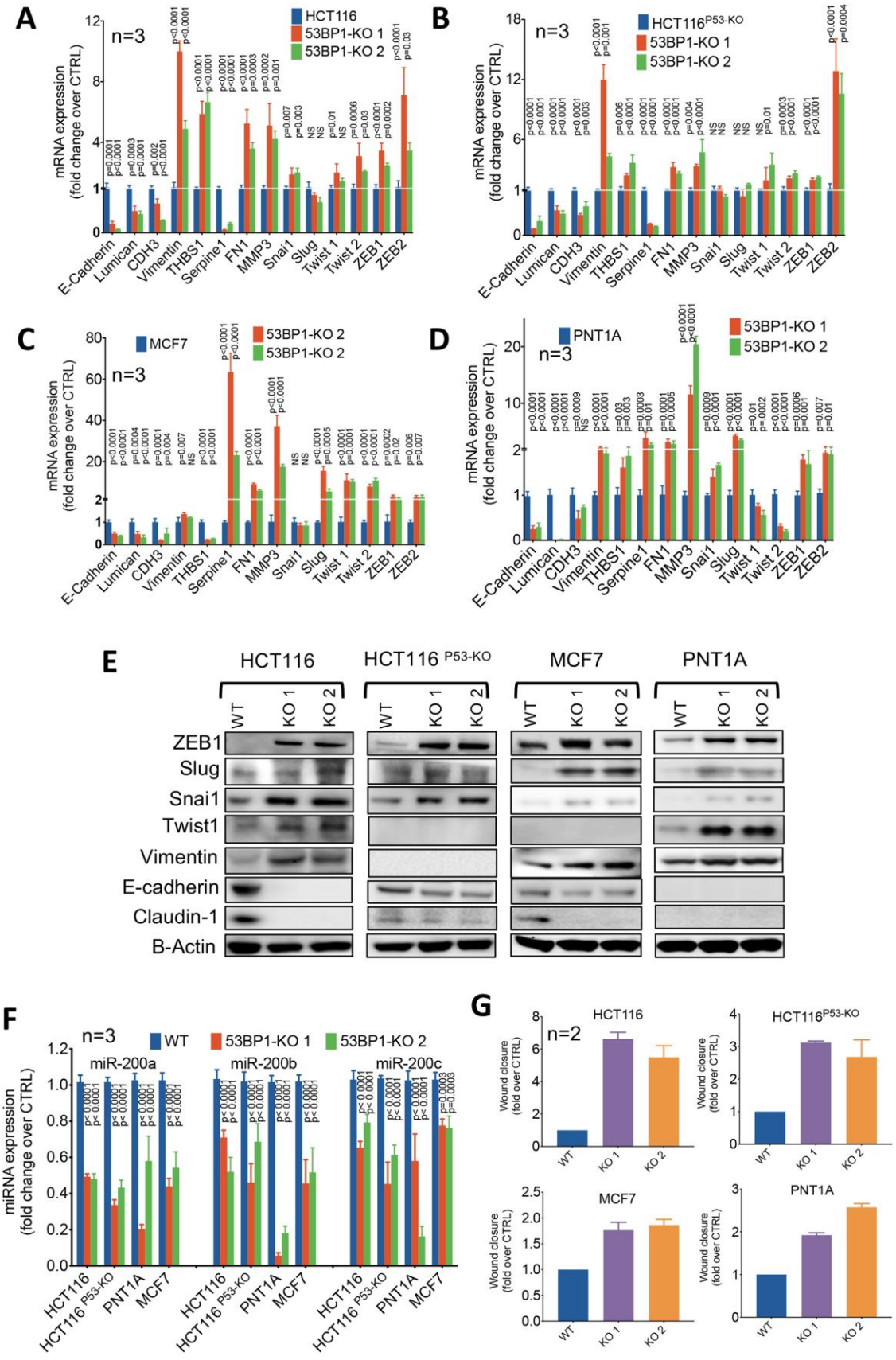

Figure 2. EMT induction following DDR attenuation is a widespread phenomenon among cancer cells.

A-D. Relative mRNA level of expression of epithelial and EMT markers in 53BP1-KO clones isolated after transfection of four different cancer/transformed cell lines: HCT116 (colon, A), HCT116P53KO (same as HCT116 but KO for P53, B), MCF7 (breast, C) and PNT1A (prostate, D). In all cases, levels are compared to the parental cell line (Dunnett's multiple comparisons test). P-values from paired comparisons are indicated. NS: non-significant. **E.** Western blot analyses evaluating the level of expression of different EMT-related markers as well as epithelial markers in all four types of cells after deletion of 53BP1. **F.** Relative expression level of three members of the miR-200 family in all four types of cells after deletion of 53BP1. **G.** Quantification of wound healing assays carried out in all four cell types before and after deletion of 53BP1. Represented are relative wound closures in KO clones with respect to the parental cell line. Measurements were made after different times (indicated in Supplementary Figure S3C where original images are presented) depending on the parental cell's wound healing capacity.

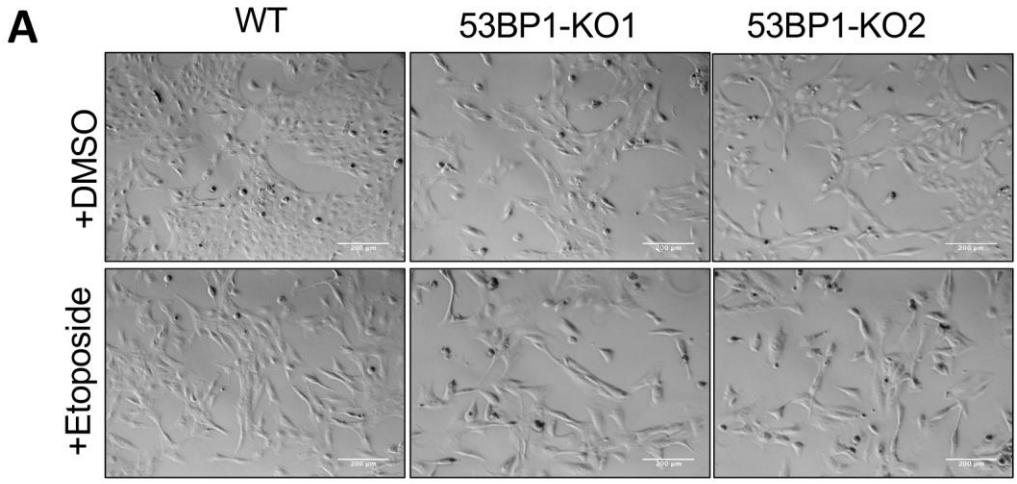
A
WT
53BP1-KO1
53BP1-KO2
+DMSO
+Etoposide

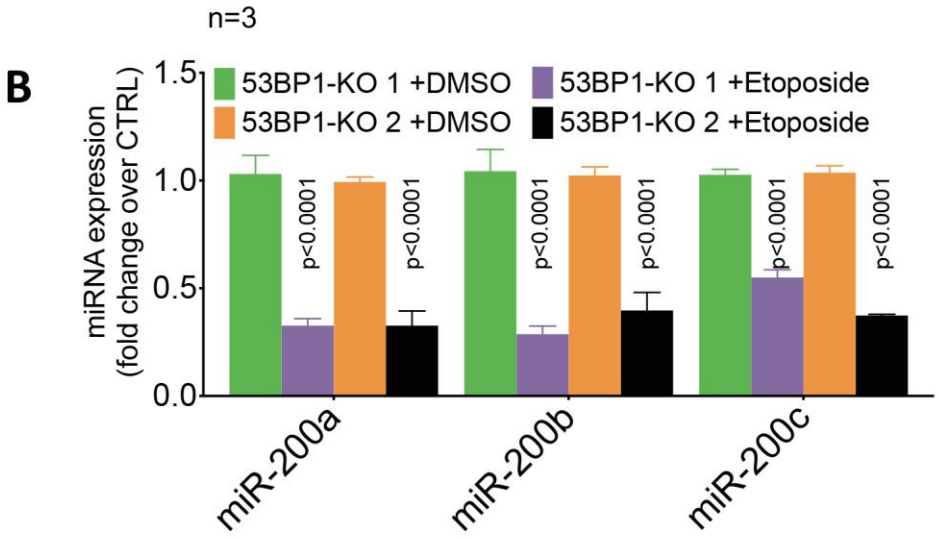
n=3
B
53BP1-KO 1 +DMSO
53BP1-KO 1 +Etoposide
53BP1-KO 2 +DMSO
53BP1-KO 2 +Etoposide
miRNA expression
(fold change over CTRL)
1.5
1.0
0.5
0.0
p<0.0001
miR-200a
miR-200b
miR-200c

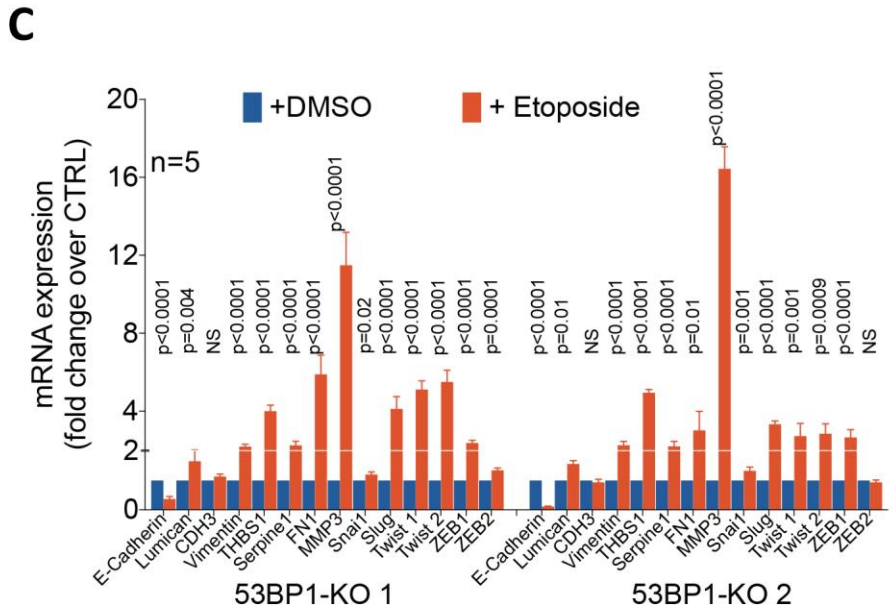
C
+DMSO
+ Etoposide
n=5
mRNA expression
(fold change over CTRL)
20
16
12
8
4
2
0
E-Cadherin
Lumican
CDH3
Vimentin
THBS1
Serpine1
FN1
MMP3
Snai1
Slug
Twist 1
Twist 2
ZEB1
ZEB2
53BP1-KO 1
53BP1-KO 2

Figure 3. Exposure to exogenous DNA damage reinforces EMT hallmarks in a DDR deficient context.

A. Cell morphology aspect of WT parental cell line and 53BP1-KO clones after treatment with etoposide 0.1µM for 7 days. Scale bar=200µm. B. Relative expression level of three members of the miR-200 family in 53BP1-KO clones after exposure to etoposide. P-values from paired comparisons (Dunnett's multiple comparisons test) are indicated. C. Relative mRNA level of expression of epithelial and EMT markers in 53BP1-KO clones after exposure to etoposide. P-values from paired comparisons (Dunnett's multiple comparisons test) are indicated. NS: non-significant.

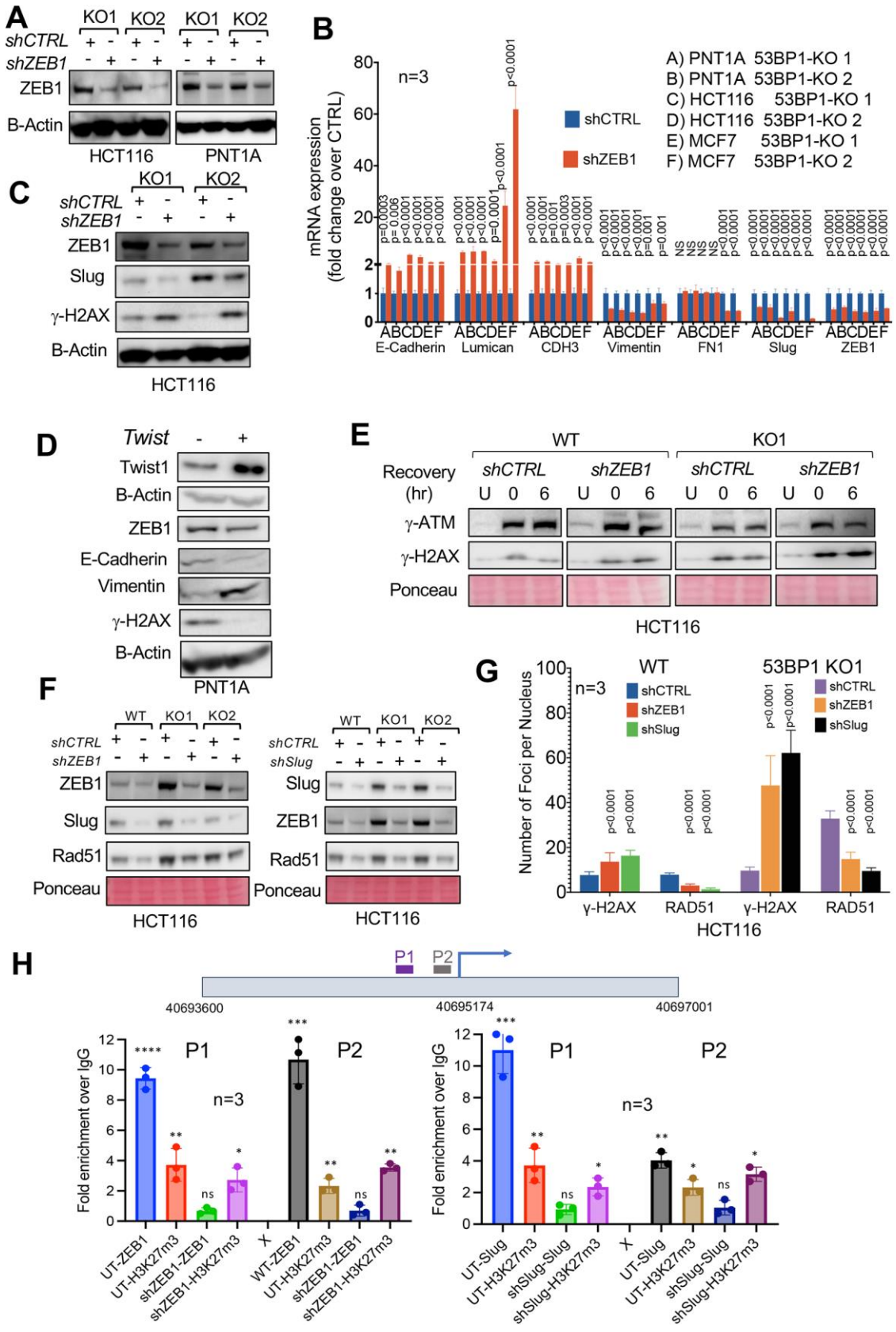

Figure 4. EMT favors DNA repair efficiency.

A. Western blot analyses for ZEB1 after introduction of a shZEB1 expressing vector into different 53BP1-KO clones. **B.** Relative mRNA level of expression of epithelial and EMT

markers in 53BP1-KO clones expressing shZEB1 as compared to the parental cell line (shCTRL). P-values from paired comparisons (Dunnett's multiple comparisons test) are indicated. NS: non-significant. **C.** Western blot analyses showing the evolution of the DNA damage marker γH2AX in HCT116 53BP1-KO clones expressing shZEB1 as compared to the control (shCTRL). Also shown are the effects of this expression on ZEB1 and Slug. **D.** Western blot analyses showing the impact on EMT markers as well as the DNA damage marker γH2AX of forced expression of TWIST1 in PNT1A cells. **E.** DNA damage recovery assay in HCT116 cells, WT and KO for 53BP1, and depleted or not for ZEB1. Cells were treated (or not, U) with etoposide (2 μM for 24h) before the medium change (0 hr) and let to recover for 6 hours. Shown here are western blot analyses for DNA damage markers P-ATP and γH2AX. **F.** Western blot analyses for ZEB1, Slug and RAD51 after introduction of a vector expressing either shZEB1 or shSlug into WT or 53BP1-KO HCT116 cells. **G.** Quantification of γH2AX and RAD51 foci detected by immunofluorescence in WT or 53BP1-KO HCT116 cells expressing either shZEB1 or shSlug. P-values from paired comparisons against the control (shCTRL) (Dunnett's multiple comparisons test) are indicated. **H.** Results from Cut&Run experiments using HCT116 cells and either anti-ZEB1 (bottom left) or anti-Slug (bottom right) antibodies for chromatin immunoprecipitation followed by enrichment analyses of two amplified DNA fragments (P1, P2) within the promoter region (ENSEMBL coordinates are indicated) of the RAD51 gene, shown here to span two small regions right upstream of the transcription initiation site (indicated by an arrow). HCT116 cells were either untreated (UT) or transduced with vectors expressing either shZEB1 (bottom left) or shSlug (bottom right). Positive control included an antibody against the histone mark H3K27me3. All PCR signals were normalized to the result obtained with positive antibody control (H3K27m3) and then to an amplified Alu fragment. Significant differences between WT, shZEB1, and shSLUG from multiple t-tests (adjusted) are indicated. *, $p < 0.05$; **, $p < 0.01$; ***, $p < 0.001$; ****, $p < 0.0001$.

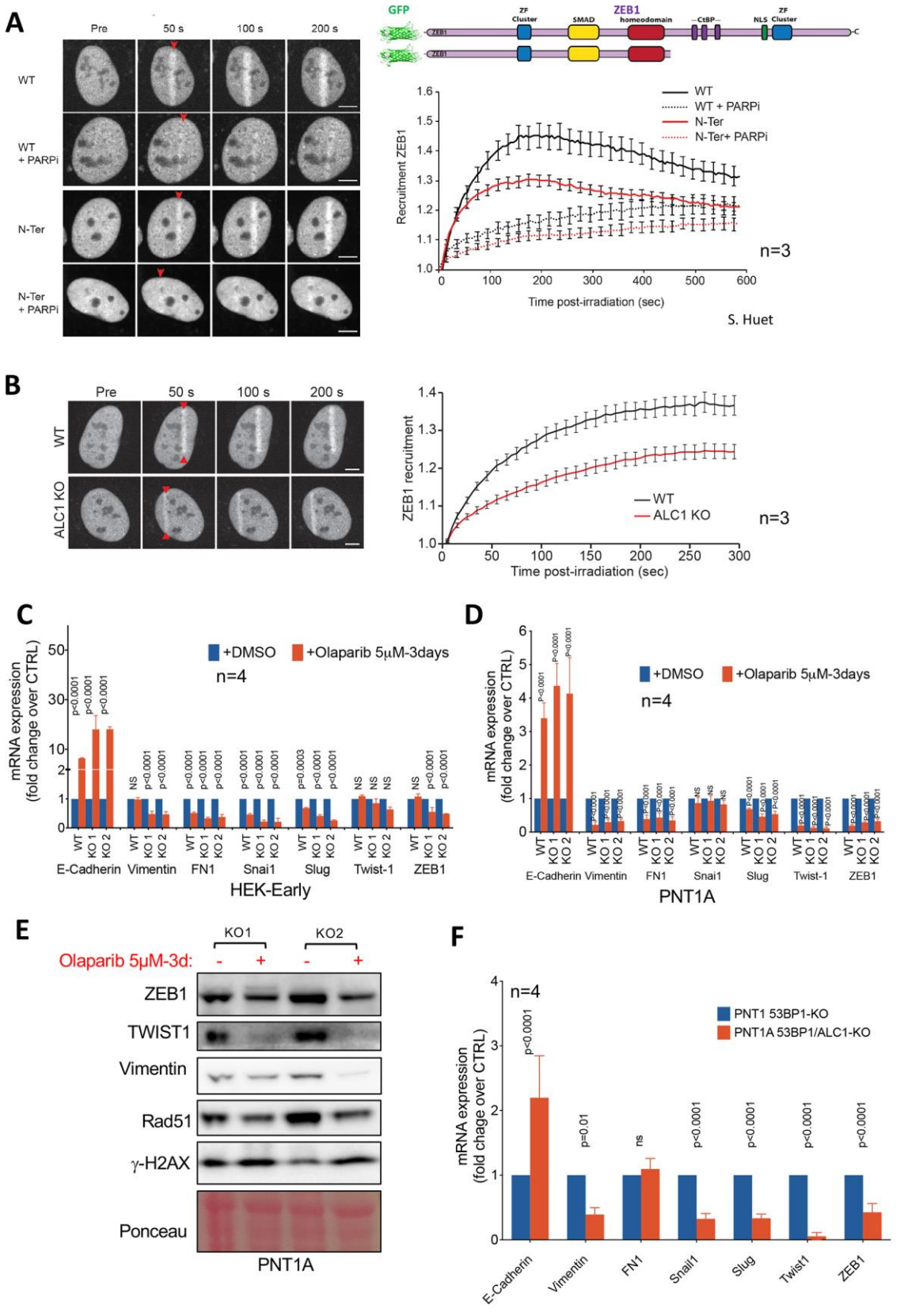

Figure 5. PARP/ALC1 are required for EMT-TF access to chromatin upon DNA damage.

A. U2OS cells expressing a GFP-ZEB1 fusion protein (either full length or deleted in its C-terminus, as shown at the top) were micro-irradiated with laser under the microscope across

nuclei and the recruitment of the fluorescent protein was followed and quantified at different time points. Cells were treated or not with Olaparib, a PARP inhibitor, at 5µM. **B.** Similar experiments were carried out with U2OS cells that had been inactivated for ALC1. **C-D.** Relative mRNA level of expression of epithelial and EMT markers in 53BP1-KO HEK-Early cells. **C.** and in 53BP1-KO PNT1A cells. **D**. treated with Olaparib at the dose and time indicated, as compared to untreated cells. P-values from paired comparisons (Dunnett's multiple comparisons test) are indicated. NS: non-significant. **E.** Western blot analyses of EMT-TFs, Vimentin, RAD51 and γH2AX in 53BP1-KO PNT1A cells before and after treatment with Olaparib. F. Relative mRNA level of expression of epithelial and EMT markers in 53BP1-KO PNT1A cells that were also inactivated for ALC1. P-values from paired comparisons (Dunnett's multiple comparisons test) are indicated. NS: non-significant.

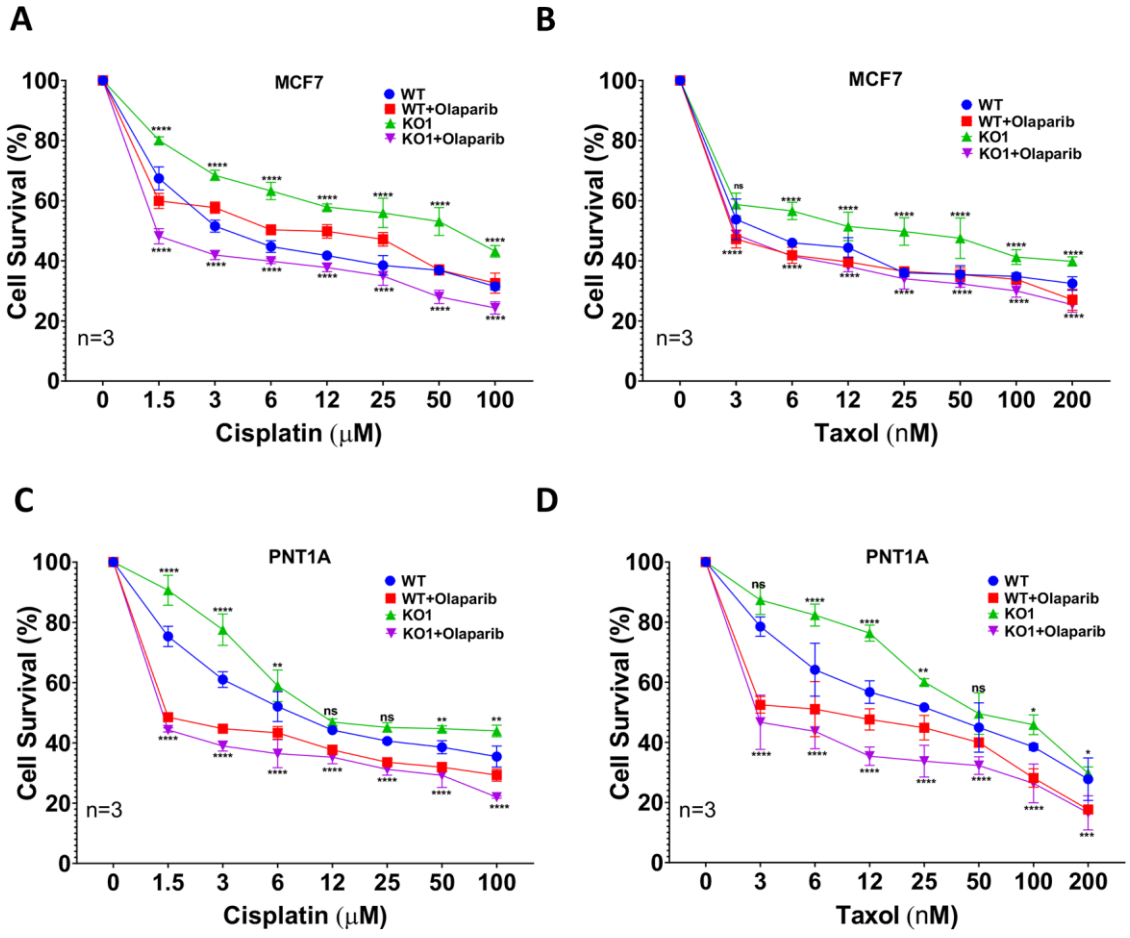

Figure 6. Olaparib restores drug sensitivity to DDR-deficient EMT transformed cells.

A-D. Cytotoxicity assays for WT and 53BP1-KO MCF7 and for WT and 53BP1-KO PNT1A cells using cisplatin or taxol, alone or in combination with Olaparib (10 µM). Significant differences from multiple t-tests (adjusted) is indicated as follows: *, $p < 0.05$; **, $p < 0.01$; ***, $p < 0.001$; ****, $p < 0.0001$.

Table 1. Expression levels of EMT transcriptional factors are positively correlated to the expression levels of RAD51 in most human cancers.

TCGA Cancer				TCGA Normal		
Cancer name	**EMT Gene**	**P-Value**	**R**	**EMT Gene**	**P-Value**	**R**
ACC (adrenocortical carcinoma)	Slug	9.2e-05	0.43	Slug	0.035	0.19
ACC (adrenocortical carcinoma)	ZEB1	0.0035	0.33	ZEB1	0.14	0.13
ACC (adrenocortical carcinoma)	ZEB2	0.00036	0.4	ZEB2	0.81	-0.021
BLCA (Bladder urothelial carcinoma)	Snail1	0.00065	0.17	Snail1	0.35	-0.23
ESCA (Esophageal carcinoma)	Twist1	0.014	0.18	Twist1	0.22	-0.36
ESCA (Esophageal carcinoma)	Slug	0.00094	0.24	Slug	0.46	-0.23
GBM (Glioblastoma multiforme)	ZEB1	2.8e-13	0.53	ZEB1	0.25	0.11
GBM (Glioblastoma multiforme)	ZEB2	0.002	0.24	ZEB2	0.6	0.051
LGG (lower grade glioblastoma)	Twist1	1.3e-13	0.32	ZEB1	0.25	0.11
LGG (lower grade glioblastoma)	ZEB1	3.7e-10	0.27	ZEB2	0.93	0.0088
LIHC (liver hepatocellular carcinoma)	ZEB1	5.3-06	0.23	ZEB1	0.91	0.017
LUAD (Lung adenocarcinoma)	Snail1	4.1e-14	0.33	Snail1	0.49	-0.093
LUAD (Lung adenocarcinoma)	Twist1	6.3-12	0.31	Twist1	0.99	0.0016
MESCO (mesothelioma)	Slug	6.7e-05	0.41			
MESCO (mesothelioma)	Twist1	0.0031	0.31			
MESCO (mesothelioma)	ZEB2	0.036	0.22			
OV (Ovary tumor)	Snail1	9.7e-07	0.23	Snail1	0.71	-0.041
PAAD (Prostate adenocarcinoma)	Twist1	3.0e-04	0.27	Twist1	0.53	-0.47
PAAD (Prostate adenocarcinoma)	Slug	7.1e-05	0.29	Slug	0.37	-0.63
READ (Rectum adenocarcinoma)	Slug	0.085	0.18	Slug	0.13	-0.51
READ (Rectum adenocarcinoma)	ZEB2	0.1	0.17	ZEB2	0.014	-0.74
SKCM (Skin cutaneous melanoma)	ZEB2	5.3e-06	0.21	ZEB2	0.38	-0.058
STAD (stomach adenocarcinoma)	Snail1	0.0028	0.15	Snail1	0.02	-0.39
TGCT (testicular germ cell tumors)	Snail1	9.9e-12	0.54	Snail1	3.3e-07	-0.38
THCA (Thyroid carcinoma)	Slug	1.3e-08	0.25	Slug	0.41	-0.11
THCA (Thyroid carcinoma)	ZEB2	4.1e-09	0.26	ZEB2	0.018	0.14
THYM (Thyoma)	ZEB1	6.2e-08	0.47	ZEB1	1	-1
UCS (Uterine carcinosarcoma)	Slug	0.022	0.3	Slug	0.33	0.11

UCS (Uterine carcinosarcoma)	Snail1	0.0061	0.36	Snail1	0.93	-0.011
UCS (Uterine carcinosarcoma)	ZEB1	0.0067	0.36	ZEB1	0.81	-0.027
UVM (Uveal melanoma)	ZEB1	4.0e-06	0.49	ZEB1	1.5e-07	-0.29
UVM (Uveal melanoma)	ZEB2	0.0073	0.3	ZEB2	0.0036	-0.16
UVM (Uveal melanoma)	Twist2	0.022	0.26	Twist2	0.012	-0.14
UVM (Uveal melanoma)	Snail1	0.043	0.23	Snail1	0.93	-0.011

RNAseq expression data was obtained from publicly available TCGA data. Comparisons were made using Spearman's correlation. P-Value and R-value are shown.